FREE AND SCATTERED ACOUSTIC FIELD PREDICTIONS OF THE BROADBAND NOISE GENERATED BY A LOW-SPEED AXIAL FAN

Korcan KUCUKCOSKUN[1], Julien CHRISTOPHE[2],
Christophe SCHRAM[2], Michel TOURNOUR[3]

[1] *École Centrale de Lyon, LMFA, 36 avenue Guy de Collongue, 69134 Ecully cedex, France*

[2] *von Karman Institute for Fluid Dynamics, 72 Chaussée de Waterloo, B–1640 Rhode–St–Genèse, Belgium*

[3] *LMS International, 68 Interleuvenlaan, 3001 Leuven, Belgium*

SUMMARY

Broadband noise generated by a low-speed industrial axial fan and its scattered field by a benchmark obstacle have been addressed. Amiet's theory on turbulence-interaction noise has been extended in order to predict the acoustic response of a fan in its geometrical near-field. A segmentation technique has been applied for spanwise varying flow conditions. The improved model has been combined with Boundary Element Method (BEM) for acoustic scattering. The validation of the broadband scattering technique has been performed through comparisons with an analytical model considering acoustic scattering from an infinite plate and with measurements of a low-speed axial fan operating nearby a flat scattering screen.

NOMENCULATURE

$\beta = \sqrt{1 - M^2}$	compressibility factor
c	chord length of the airfoil
c_0	speed of sound
d	semi-span length of the airfoil
g	airfoil pressure distribution for a sinusoidal gust
kc	acoustic wave number normalized by the chord
k_y	spanwise acoustic wave number
p	acoustic pressure at the observer
ρ_0	density of the medium
σ	propagation distance
σ_t	far-field approximation for the propagation distance

$\sigma_\varkappa$	spanwise geometrical near-field approximation for the propagation distance
t	time
v_n	incident acoustic normal velocity on the solid surface
ω	radian frequency
x, y, z	acoustic element positions with respect to the airfoil center
x_0, y_0	positions of dipoles on the airfoil surface
B	number of blade
$Fe^{i\omega t}$	source strength of a dipole
$K_x = \omega/U$	particular chordwise acoustic wave number
$K_y = \omega y/c_0\sigma$	particular spanwise acoustic wave number
$\mathcal{L}$	aeroacoustic response function for a gust
Λ	integral length scale of turbulence
M	impinging mean flow Mach number in the positive chordwise direction
Ω	rotational speed
Φ_{ww}	power spectrum of the upwash velocity component
ψ	azimuthal position of the blade strip
Spp	acoustic pressure PSD
Spv, Svp, Svv	acoustic pressure-acoustic velocity PSD
U	impinging mean flow velocity in the positive chordwise direction

INTRODUCTION

The aerodynamic noise generated by low-speed fans is a concern in many industrial applications in terms of comfort and regulations. In the energy sector the noise emitted from wind turbine blades may be inconvenient for the inhabitants. In the transportation industry, the noise generated by cooling fans may result annoyance for passengers.

The aeroacoustic response of fans is investigated in tonal and broadband branches. The former is due to periodic forces acting on blades. It appears at discrete frequencies such as the Blade Passing Frequency (BPF) and its higher harmonics [1-3]. The latter results from random force fluctuations acting on blades, due to turbulence-interaction or development of turbulent boundary layer (TBL) on the blade surface [4] for example. If a fan is operating in a low-turbulent flow-field, development of TBL and its interaction with the trailing edge results in broadband self-noise. Several works have been performed in order to predict the self-noise analytically and experimentally [5-7]. Furthermore, if the impinging flow is highly disturbed, the turbulence-interaction noise becomes dominant [8,9]. Due to installation effects, the source of the broadband noise generated by an axial cooling fan located in the automotive engine mostly results from the interaction between the fan and incoming turbulent flow. This paper deals with prediction of broadband noise generated by interaction of fan blades with turbulent flow.

In order to predict the acoustic response of a stationary airfoil located in a turbulent stream a theory has been proposed by Amiet [10]. Accounting for rotational effects, this model was extended by Paterson and Amiet and applied for prediction of the noise emitted by a helicopter rotor [8]. One of the main assumptions made in Amiet's formulation is consideration of an observer located in acoustic and geometrical far-field, hence an analytical solution can be obtained. In this paper, an intermediate level of correction is taken into account considering observers located in geometrical near-field with respect to the spanwise extent of the airfoil [11]. Another hypothesis involved in the derivation of the theory is the assumption of homogeneous turbulent flow-field impinging onto the linearized airfoil. Statistically homogenous turbulent models, such as von Karman or Liepmann, can

be used in order to model the incoming turbulence spectrum in such cases. However, fan blades are usually subjected to spanwise varying incoming turbulent flow conditions due to the rotation and installation effects. The blade is then divided into short strips in the spanwise direction and each strip could then be considered in homogeneous turbulence [11-14]. But this approach can neglect the effect of the large hydrodynamic wavelengths impinging onto the short strips. In this paper an alternative segmentation method considering the effect of the large wavelengths is employed [13].

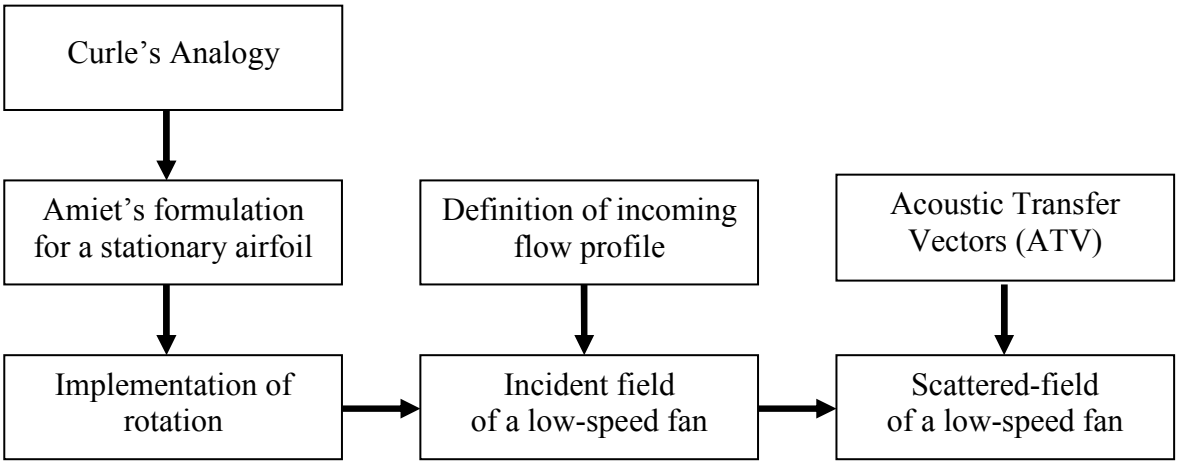

Figure 1. Flowchart of the fan noise simulation

Another key point addressed in this paper is the scattering of broadband noise generated by low-speed fans. Acoustic free-field propagation can be assumed for the certification of wind turbines, however for an automotive cooling fan, acoustic scattering by surrounding surfaces of the cooling unit has to be considered. In order to calculate the sound propagation and scattering by surrounding surfaces, several theories have been proposed such as Helmholtz solvers, based on the Finite Element Method (FEM) or Boundary Element Method (BEM) [15], and more sophisticated methods based on the resolution of Linearized Euler Equations which are already in use in industry [16]. A common denominator of these techniques is the requirement of the deterministic definition of the source field. However, due to the statistical description of turbulence, the phase information in the source term is lacked. A formulation based on the auto- and cross-power spectra of the acoustic field, calculated through the extension of Amiet's theory combined with a BEM concept is therefore employed [11,17]. Figure (1) shows the flowchart of the fan noise simulation employed. This approach is applied to compute the scattered field of the broadband noise generated by a low-speed axial fan operating nearby a benchmark flat scattering screen [18].

GENERALIZATION OF AMIET'S THEORY

Acoustic response of an airfoil placed in a turbulent stream consists of radiation of chordwise and spanwise distributed point dipoles on the airfoil surface which is assumed to be with zero thickness, camber and angle of attack. The acoustic far-field pressure generated by a point dipole is given by Curle [19] as

$$\mathrm{p(x,y,z,\omega;x_0,y_0)} = \frac{i\omega F(x_0,y_0)e^{i\omega t}}{4\pi c_0 \sigma_t^2}\,\mathrm{e}^{-\mathrm{i}\omega\sigma_\mathrm{t}/\mathrm{c_0}} \tag{1}$$

neglecting acoustic near-field terms. The propagation distance σ_t accounting convection effects is defined as

$$\sigma_t = \left(\sqrt{(x-x_0)^2+\beta^2(y-y_0)^2+\beta^2 z^2} - M(x-x_0)\right)/\beta^2 \tag{2}$$

where are the coordinates of the observer with respect to an origin located at the center of the airfoil surface as shown in Figure (2). are the chordwise and spanwise positions of the point dipoles on the linearized airfoil surface. and are the angular frequency and the speed of sound, respectively. is the Mach number of the uniform flow in the positive *x*-direction, and is the compressibility factor. The source strength of the wall-normal dipole, is obtained from the distribution of the lift across the airfoil swept by a skewed sinusoidal gust.

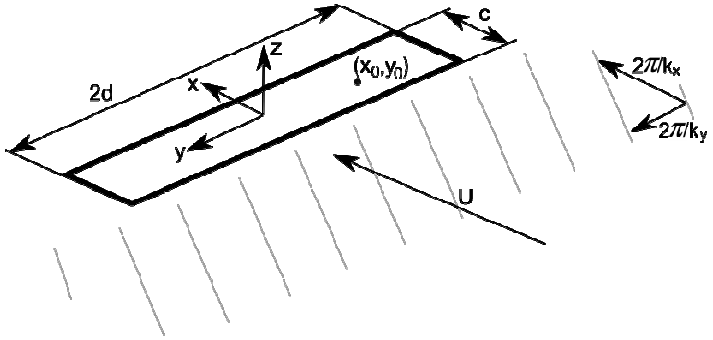

Figure 2. A sketch of an airfoil swept by a skewed gust

Integrating explicitly the distribution of dipoles over the airfoil surface of span and chord for both chordwise and spanwise wave numbers yields the following expression for the acoustic PSD

(3)

where is the response function linking the incoming gust to the lift on the surface. Only one chordwise wave number emerges in the Fourier domain, . The superscripts and * represent the second integral variable and the complex conjugate operator, respectively. is the power spectrum of the incident upwash velocity component. This formulation is valid for any observer position but in acoustic far-field of the airfoil. One of the hypotheses in the final formulation of Amiet's theory for turbulence-interaction noise is that considering an observer located in geometrical far-field, such that Equation (2) is simplified to [10]

(4)

The sound power spectral density (PSD) at the far-field can then be expressed as [10]

(5)

where is the aeroacoustic transfer function given, e.g. by Paterson and Amiet [8] and extended by Graham [20]. However, in many industrial applications, scattering of the sound emitted by fan blades for example, acoustic quantities used for scattering computation have to be obtained at a short distance from the considered blade. The first key aspect of the present paper is generalization of Amiet's theory [10] for a listener at a distance from the blade which can become similar to its span-length, defined as the spanwise geometrical near-field [11].

Spanwise Geometrical Near-Field Correction

For large-span airfoils and for source-observer distances similar to the spanwise extent, assuming that can be reasonable, whereas may consist in a gross approximation. An intermediate level of approximation for low-Mach number flows is therefore introduced as

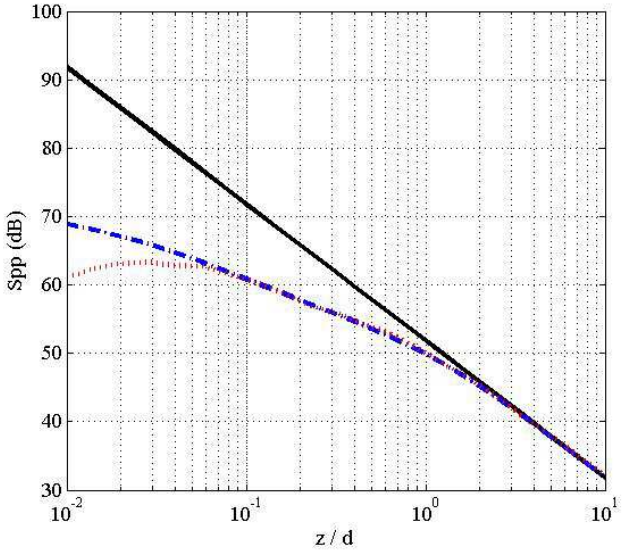

Figure 3. Comparison of acoustic spectra at various distances, using Amiet's model (5) (plain), direct integration (3) (dots) and geometrical near-field correction (7) (dash-dots) for U = 30 m/s, TI = 0.05m, Λ = 0.009 m.

$$\sigma_t \sim \sigma_\varkappa = \sqrt{x^2 + \beta^2(y-y_0)^2 + \beta^2 z^2}. \tag{6}$$

Considering this approximation, the PSD of the airfoil in its spanwise geometrical near-field reads [11]

$$Spp(x,y,z,\omega) = \left(\frac{\omega\rho_0 z}{2c_0}\right)^2 U \int_{-\infty}^{\infty} \left|\varkappa(x,y,z,K_x,k_y)\right|^2 \left|\mathcal{L}(x,K_x,k_y)\right|^2 \Phi_{ww}(K_x,k_y)\, dk_y. \tag{7}$$

The new solution differs from the classical solution of Amiet, Equation (5), by the modified function $\varkappa$, defined as a combination of Exponential integrals E_1 [21] as

$$\begin{aligned}\varkappa(x,y,z,\omega,K_y,k_y) = {} & \frac{ie^{i(K_y+k_y)y}}{2\beta^2\sqrt{x^2/\beta^2+z^2}} \\ & \{e^{-(K_y+k_y)\sqrt{x^2/\beta^2+z^2}}\, E_1\left[-(K_y+k_y)\sqrt{x^2/\beta^2+z^2} - i(K_y+k_y)(d-y)\right] \\ & -e^{-(K_y+k_y)\sqrt{x^2/\beta^2+z^2}}\, E_1\left[-(K_y+k_y)\sqrt{x^2/\beta^2+z^2} - i(K_y+k_y)(-d-y)\right] \\ & -e^{(K_y+k_y)\sqrt{x^2/\beta^2+z^2}}\, E_1\left[(K_y+k_y)\sqrt{x^2/\beta^2+z^2} - i(K_y+k_y)(-d-y)\right] \\ & e^{(K_y+k_y)\sqrt{x^2/\beta^2+z^2}}\, E_1\left[(K_y+k_y)\sqrt{x^2/\beta^2+z^2} - i(K_y+k_y)(-d-y)\right]\}.\end{aligned} \tag{8}$$

First, a test is performed in order to compare the results provided by the far-field formulation (5) the spanwise near-field expression (7), and a direct numerical integration of Equation (3) using a Monte Carlo integration method [11]. Figure (3) shows the PSD of a stationary airfoil subjected to homogeneous turbulence properties, at various distances z on the line $(x,y) = (0,0)$ at a fixed frequency, $kc = 1.2$. A von Karman model is selected for the turbulent energy spectrum with an incoming velocity $U = 30m/s$, a turbulence intensity $T.I = 0.05$, and a turbulent length scale $\Lambda = 0.009$ m [22]. The airfoil chord is fixed to $c = 0.13m$, and a large-aspect ratio airfoil is assumed by using a span $2d = 40c$ [11]. Dots, plain and dash-dots represent formulations (3), (5) and (7), respectively. All formulations converge asymptotically at $z > 2d$, addressing the limit of application of the geometrical far-field formulation (5) where $z = 2d$ corresponds to the size of the spanwise extent of the airfoil. The spanwise near-field expression (7) shows a good agreement with

the general formulation (3) up to $z < 0.08d$ and highly improves the solution compared to the far-field solution (5) of Amiet's. The deviation at $z < 0.08d$ can be addressed as the chordwise geometrical near-field effects.

Figure 4. Experimental facility in the anechoic chamber, wind tunnel-optimized airfoil configuration

Experiments have been conducted for comparison of the measured acoustic PSD with the broadband noise predictions in free-field. A thin (relative thickness less than 3%) and slightly cambered optimized airfoil is mounted downstream of a wind tunnel in the anechoic chamber of the École Centrale de Lyon as seen in Figure (4). The dimensions of the room are $6 \times 5 \times 4m^3$, and walls, floor and ceiling are covered with acoustic absorbing material. The cut-off frequency of the room is $100Hz$. A 0.5 inch dimater B&K 4189-A-021 microphone with an optimized frequency response range of 20 Hz to 20 kHz has been used. Its dynamic range with preamplifier is between 16.5 dBA to 138 dB. The isolated airfoil has 2.3c span with $\mathrm{c} = 0.13\mathrm{m}$. The jet nozzle is rectangular with an outlet size $2.3\mathrm{c} \times 1.2\mathrm{c}$. The airfoil is placed at zero angle of attack with its leading edge. The jet exhaust Mach number is $\mathrm{M} = 0.09$. In order to create isotropic and homogeneous turbulence impinging to the leading edge of the airfoil, a square grid is placed upstream of the nozzle. The turbulence generated by the grid-nozzle mock-up at the impingement line includes a turbulence rate of 5% and an integral length scale Λ of 0.009 m as used in the numerical comparison above [22]. A von Karman model is again selected for the turbulent energy spectrum. Figure (5) shows the comparison of the acoustic field emitted by the airfoil for observer positions at $10/3$ and $4/3d$ away from the airfoil on the mid-plane. The measurements, solution (5) and the solution (7) are represented as black plain, dashed and red plain, respectively. A very good agreement is obtained between the measurements and the semi-analytical solutions at the frequency range of $500 - 10000$ Hz where the differences between two spectra are less than 5 dB. A possible explanation of the discrepancies between the predictions and the measurements at low frequencies might be related to the defects in the flow-field measurements. Additionally, the general formulation (3) neglects the acoustic near-field effects, which may contribute to the sound field at the lowest frequencies. However, the humps and dips in the spectral shape due to the non-compactness of the airfoil are well captured at higher frequencies. As seen in the figure (left), the solutions (5) and (7) converge at the far-field. However, for the observer located in the spanwise geometrical near-field of the airfoil (z/d=4/3 here), the solution (7) provides a better agreement with the measurements at higher frequencies compared to the solution (5), where the improvement between two solution is around 2 dB. Since Equation (7) is attractive for geometrical near-field computations due to its accuracy and robustness for listener positions further than the airfoil chord, it will then be used in the following sections involving rotation and scattered-field computations.

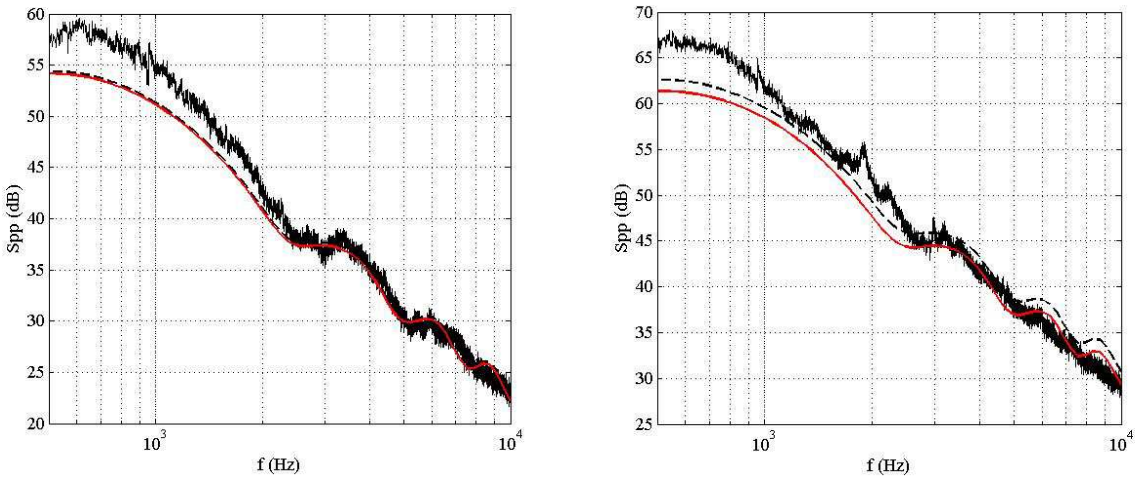

Figure 5. Acoustic spectra of the optimized airfoil at z=10/3d (left) and z=4/3d (right). Measurements (thin) geometrical near-field expression (7) (red) and far-field expression (5) (dashed) for U = 15 m/s, TI = 0.05, Λ = 0.009 m.

Additionally, the theory proposed by Amiet is based on the assumption of uniform and homogenous turbulent stream impinging to the airfoil. However, the incoming flow is not uniform in most of the industrial applications; such the impinging velocity onto blades varies proportionally with the radius due to rotation. One approach proposed in order to take the spanwise varying incoming flow conditions into account is splitting the airfoil into small strips assuming the flow impinging on each strip is uniform and homogenous. The total PSD of the airfoil is then obtained through a summation of PSD of each individual strip –named as classical strip method [8,11]. However, small strips are not able to capture large spanwise hydrodynamic wavelengths. The total PSD therefore underpredicts the acoustic field at lower frequencies. Hence, the segmentation following the inverse strip method proposed by Christophe [23] is employed. The PSD of each small strip is now computed with a subtraction of the PSD of a truncated airfoil from the one of the initial large aspect ratio airfoil. The difference of the span-lengths is equal to the span-length of the particular strip. Both airfoils are assumed to be in homogeneous stream. The subtraction therefore leads to include the effects of large hydrodynamic wavelengths.

Implementation of rotation

The theory of turbulence-interaction noise for a stationary airfoil [10] has been extended for low speed rotor blades [8]. The stationary airfoil model has been applied to each blade strip where the circular motion is replaced by the locally tangential translation motion which is only acceptable at sound frequencies much higher than the rotational frequency, $\omega \gg \Omega$. For both free and scattered-field computations, the observer and acoustic mesh position is defined in the fixed reference frame with respect to the rotation plane and the rotation axis. As mentioned in the isolated airfoil theory above it is required to define the origin in a fixed reference frame with respect to the blade strip in order to predict the acoustic response of the strip using Equation (7). A coordinate transformation is therefore performed taking the geometry of the blade into account including sweep, pitch and twist angles [18,24]. The impinging velocity onto the blade strip is then the vector summation of the tangential velocity, $U = \Omega r$, and the axial velocity concerning the pitch angle of the blade strip [24].

Due to the relative motion between the source and the observer, the emitted frequency from the blade strip and the observed frequency are not equal. The ratio of the frequencies is linked by the Doppler factor [8]. However, for a low-speed axial fan, the Doppler effect was shown to be negligible and the observed frequency converges to the emitted frequency [25]. In the present work the maximum Mach number is less than 0.15, hence Doppler effect becomes negligible. Assuming

the same gust has not been cut by succeeding blades [8], the free-field PSD of a low Mach number axial fan with B blades is computed with the integration on the azimuthal positions [18] of the blade ψ as,

$$Spp(X,Y,Z,\omega) = \frac{B}{2\pi}\int_0^{2\pi} Spp^{\psi}(x,y,z,\omega)d\psi. \quad (9)$$

Broadband Scattering

The configurations described below involve low-Mach number axial fans placed in a turbulent field and in presence of scattering surfaces. In the present scattered-field approach, the acoustic pressure field is first decomposed into incident and scattered components: $p = p_i + p_s$. On one hand, the free-field response of the fan p_i can be obtained from the approaches described above. On the other hand, the scattering problem is solved by means of BEM formulation [26]. The broadband noise model used is based on a statistical description of the source field. The deterministic BEM problem is therefore re-formulated employing the Acoustic Transfer Vector (ATV) concept [11,15,17]. ATVs link the scattered acoustic pressure at a listener point to the wall-normal component of the incident acoustic velocity of the boundary elements on the scattering surface

$$p_s(\omega) = \{ATV(\omega)\} \cdot \{v_n(\omega)\}. \quad (10)$$

Normal velocities $\{v_n(\omega)\}$ correspond to opposite of the projection of the incident velocity field, so that the summation of the scattered and incident fields satisfies the rigid Neumann boundary condition on the scattering surface [26]. The incident velocity $\{v_i(\omega)\}$ can be computed by the gradient of the incident pressure obtained via expression (1). The same acoustic far-field assumption therefore applies to the position of the scattering surface, as for the listener position. The total acoustic PSD finally reads [11,18]

$$Spp_t = Spp_i - Spv \cdot \boldsymbol{ATV}^{\boldsymbol{T}} - \boldsymbol{ATV}^{*} \cdot Svp + \boldsymbol{ATV}^{*} \cdot Svv \cdot \boldsymbol{ATV}^{\boldsymbol{T}} \quad (11)$$

where Spp_i is the incident acoustic PSD at the listener points in free-field. Spv and Svp are the cross-power spectra of the velocity evaluated over the acoustic mesh and acoustic pressure at the listener points. Finally Svv is the auto- and cross-power spectrum of the velocities over the acoustic mesh. The superscripts * and ^{T} stand for the complex conjugate and transpose operators, respectively. $\boldsymbol{ATV}(\omega)$ is finally a matrix composed for each listener point and acoustic elements computed with LMS software Virtual Lab. and Sysnoise [15].

VALIDATION

The scattered-field approach described above is implemented in both analytical and experimental validation cases. The former assumes a modelS case where the fan is located parallel to a finite scattering plate in absence of an upstream flow. The latter compares the computed acoustic spectra with the measurements performed in an anechoic chamber.

Image Method

A theoretical comparison is performed considering a low-speed axial fan with 4 blades [18]. The rotational speed of the fan is selected as, $\Omega = 3000rpm$. The tip and hub Mach number are equal to 0.08 and 0.15, respectively. The blade is split into 4 spanwise strips and all strips are linearized. The chord-lengths of the strips are fixed along their span. Turbulent parameters, such as the turbulence intensity and the turbulent length scales are assumed not varying in the spanwise direction and selected as 20% and 0.005 m, respectively [18]. For the testcase, spanwise variation of the incoming flow is only taken into account in the impinging velocity which is a function of the rotational speed, radius and pitch angle of the blade strip [24].

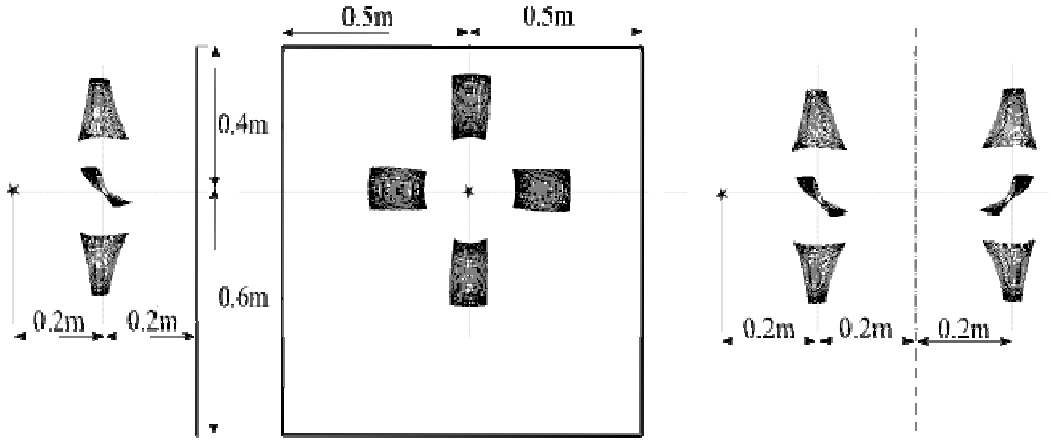

Figure 6. Sketches of the scattering problem, ATV model (left) and Image Method (right)

A low-speed axial fan operating across a flat screen which is parallel to the rotation plane is considered. Since the turbulence-interaction noise prediction is based on dipole distribution on the blades, the parallel placement of the fan and screen maximizes the effects of the scattered acoustic field. A screen is used in the comparisons. The observer is located on the rotation axis at m above the fan [18]. The screen is mounted m away, parallel to the rotation plane but on the other side of the fan with respect to the observer as seen in Figure (6).

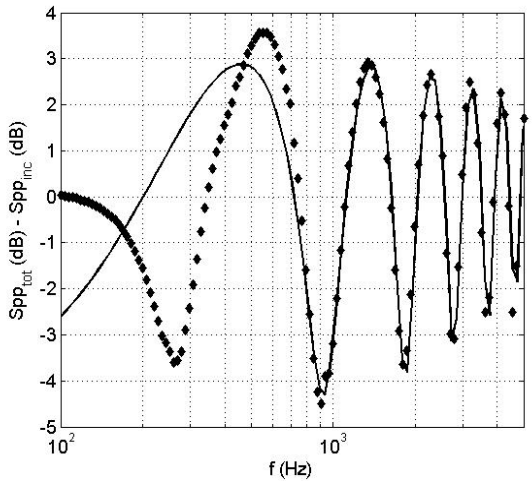

Figure 7. Difference between the total and free-field spectra for the benchmark axial fan. Image Method (plain) and ATV model (symbols). Observer is located at 0.2m away on the rotation axis, plate is located perpendicular to the rotation plane, at 0.2m away from the rotation center.

Scattering by the flat screen is calculated with two different models; first with the image method, secondly with the ATV method described above. The former assumes the flat screen is infinite and is replaced with a phase shifted image fan symmetrical to the screen. However, this case is ideal and neglects the effects of the sound waves scattered by the free edges of the finite screen. Furthermore, the latter takes the finite extent of the screen into account and it can be used with arbitrary geometries since it is based on BEM formulation. Figure (7) shows the difference between the total and incident field spectra in terms of dBs. Both the image (plain) and ATV (symbols) methods converge above Hz showing the accuracy of the implementation. The ATV model captures one additional deep at lower frequencies, which can be addressed as the scattering of the large wavelengths by the free edges of the obstacle [11].

Experimental Validation

A set of experiments is performed in the anechoic chamber at École Centrale de Lyon [18]. A low-speed axial fan running next to a flat plate is investigated shown in Figure (8) (left). The rotor has 3 uniformly distributed blades and it rotates at 1200rpm. The Blade Passing Frequency (BPF) is then equal to 60Hz. The tip Mach number is around 0.08 satisfying the low-speed fan assumption. Since the theory described above is related to turbulence-interaction noise, the rotor is operated in presence of an upstream turbulent flow. This is achieved by running the rotor at the outlet of a nozzle where the flow is disturbed by an upstream square grid. The rotation plane is located 3 radii downstream of the nozzle outlet. The jet exhaust velocity is fixed to 15 m/s. The measurements are taken at 3 radii away from the rotation center and 2.5 radii away from the rotation axis in order to avoid the pseudo sound [18].

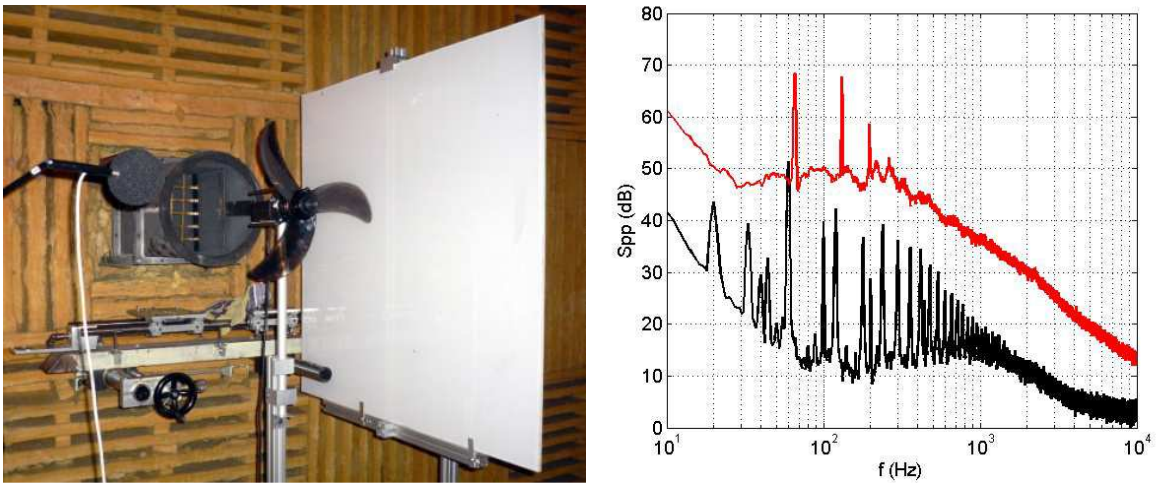

Figure 8. Low-speed axial fan in the anechoic chamber (left). Acoustic PSD without (black) and with (red) turbulent flow at z=3r. (right) [18].

Figure (8) (right) shows the acoustic spectra of the rotor in free-field with (red) and without (black) presence of incoming turbulent flow. The tonal component of the fan is dominant in the entire spectrum in absence of turbulence. However, in presence of the upstream turbulent flow, the broadband component becomes dominant. Since the difference between the both spectra is well significant, the sound emitted by the fan can be considered as turbulence-interaction noise. Hence the model described above can be employed. In order to obtain the description of the source-field, the turbulent-flow field on the rotation plane is measured using a hot-wire anemometer [18]. The measurements are taken on a line starting from the center of the jet axis till the tip radius of the fan. Once the turbulent spectrum is measured at a given location, the turbulent length scale is then obtained by fitting the von Karman model to the measured one using the measured flow parameters [22]. Figure (9) (left) shows the measured spectra (plain) at the center of the strips and the superimposed von Karman spectra (dotted). The plots are shifted by steps of 10 dB for clarity. The slope of the spectra fits with the $-5/3$ power law, hence the turbulent flow can be locally assumed isotropic and homogeneous [27] for the present configuration. All the turbulent flow parameters used are shown in Figure (9) (right) with respect to the radial position of the probe. The mean flow velocity and the turbulent length scales are non-dimensionalized with the jet core velocity and the tip radius of the fan, respectively.

The blade is split into 4 spanwise segments using inverse strip theory and the von Karman model spectrum is selected for the predictions [18]. Measured and computed free-field spectra of the fan are shown in Figure (10) (left). The red line represents the measured one where the line-dots shows the one obtained using the model described above. A very good agreement is observed with the measurements and the numerical model above 400Hz. The disagreement at the lowest frequencies

can be due to additional sound sources since the fan is operating at off-design conditions. Hence, the model described above is shown to be an efficient tool to predict the free-field of an axial fan due to turbulence-interaction and it will be used for the scattered-field computations.

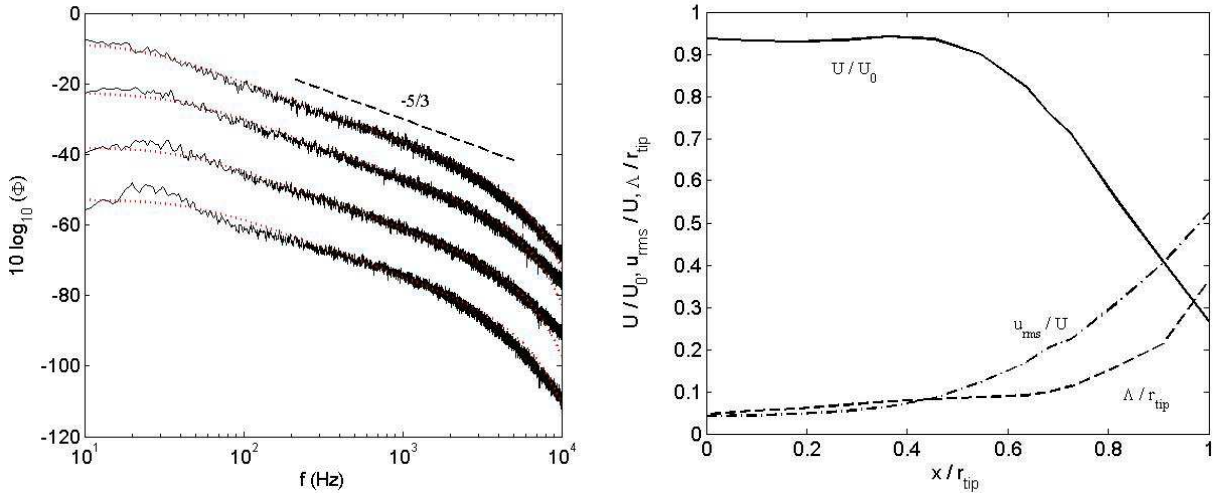

Figure 9. Turbulence spectra at the strip centers on the rotation plane (left) measured (plain) and fitted von Karman model (dots) and corresponding flow profile (right) normalized velocity (plain), turbulent intensity (dash-dots) and modeled turbulent length scale [18].

A 1m×1m plexiglass flat screen is introduced perpendicular to the rotation plane as seen in Figure (8) [18]. The screen is located at 1.5 radii away from the rotation axis. The selected distance of screen is far enough as not to disturb the incoming flow. Figure (10) (right) shows the difference between the total and incident field spectra. The red line represents the measurements. Symbols stand for the semi-analytical model described above combined with inverse strip theory and ATV approach. The interference fringes due to the scattering screen are well captured above 400Hz. The difference with the measurements is less than 1 dB at corresponding frequencies. The disagreement at the lowest frequencies may be due to the scattering of the other source mechanisms as mentioned above [18]. Finally, using the inverse strip theory, both total and incident field spectra given in the related reference [18] have been improved around 2 dB below 1kHz.

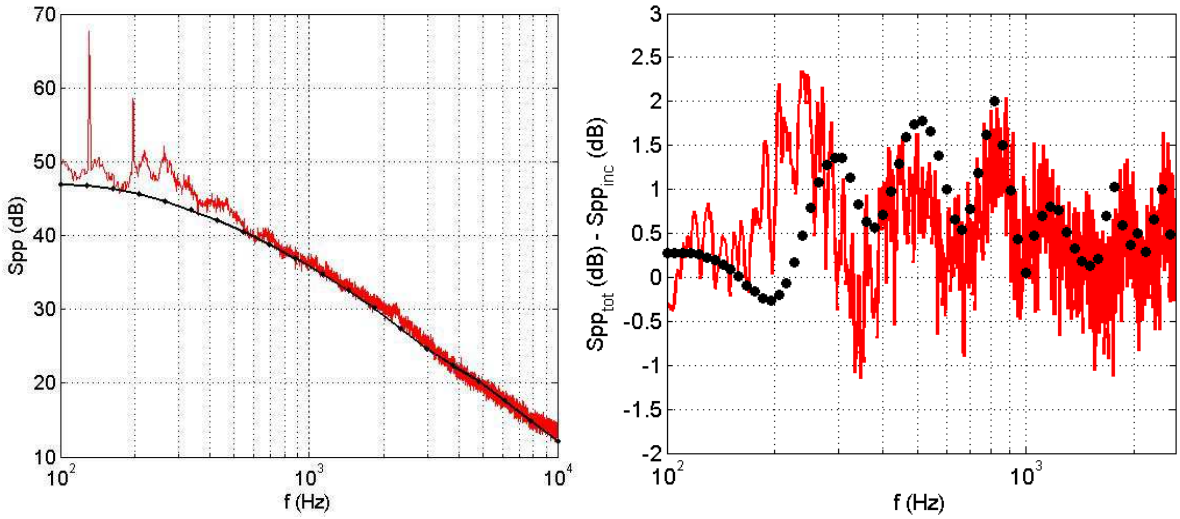

Figure 10. Acoustic free-field spectra (left) at z=3r measured (red) and semi-analytical model with 4 spanwise segments using inverse strip theory (black). Difference between total and free-field spectra (right). Measurements (line) and semi-analytical model combined with inverse strip theory and ATV approach (symbols).

CONCLUSIONS

Broadband noise emitted by low-speed axial fans due to turbulence-interaction is an important issue for industrial applications. Amiet's theory has been used by several authors in order to deal with this problem for configurations in free-field. The present paper considers industrial fan problems where the reflection and scattering by surrounding surfaces are significant.

The theory based on far-field assumption is first extended in order to take the geometrical near-field effects into account. Further, the spanwise-varying incoming flow field is considered with inverse strips theory. A good agreement is obtained in the acoustic free-field predictions using an industrial low-speed axial cooling fan operating in a turbulent stream and measurements performed in an anechoic chamber.

A method based on ATV approach is employed in order to compute the scattered broadband noise of a fan. It is first validated against an analytical model. A very good agreement is observed in the model comparisons. Finally the scattered-field prediction of the low-speed industrial axial fan is compared with the measurements performed in an anechoic room using a benchmark scattering screen. A good agreement is observed in comparison with experimental data. The interference fringes due to the scattering are well captured using the ATV approach at the frequencies of interest.

The analytical model proposed is limited with low Mach number fan noise applications. However, the model combined with ATV method is found to be a useful tool for realistic scattering problems of broadband fan noise including arbitrary geometries.

ACKNOWLEDGEMENTS

This work is supported by European Commission in the framework of the FP7 Collaboration Project ECOQUEST (grant agreement no 233541). The authors are thankful to Prof. Michel Roger for fruitful discussions.

REFERENCES

[1] J. E. Ffowcs Williams, D. L. Hawkings – *Sound Generation by Turbulence and Surfaces in Arbitrary Motion*, Philosophical Transactions of the Royal Society of London. Series A, Mathematical and Physical Sciences 264, 1151:321-342, **1969**

[2] M. Goldstein – *Aeroacoustics*, McGraw–Hill Inc., **1976**

[3] M. Roger – *Near-Field Fan Noise Modeling and Installation Effects Due to Scattering Surfaces*, Proceedings of Fan Noise conference, Lyon, **2007**

[4] S. Moreau, M. Roger – *Competing Broadband Noise Mechanisms in Low Speed Axial Fans*, AIAA Journal 45 (1):45-57, **2007**

[5] M. S. Howe – *A Review of the Theory of Trailing Edge Noise*, Journal of Sound and Vibration 61 (3):437-465, **1965**

[6] T. F. Brooks, M. A. Marcolini, D. S. Pope – *Airfoil Trailing Edge Flow Measurements*, AIAA Journal 24 (8):1245-1251, **1986**

[7] Y. Rozenberg, M. Roger, S. Moreau – *Rotating Blade Trailing-Edge Noise: Experimental Validation of Analytical Model*, AIAA Journal 48 (5), **2010**

[8] R. W. Paterson, R. K. Amiet – *Noise of a Model Helicopter Rotor due to Ingestion of Turbulence*, NASA, TR-CR 3213, **1979**

[9] T. Carolus, M. Schneider, H. Reese – *Axial Flow Broad-band Noise and Prediction*, Journal of Sound and Vibration 300:50-70, **2007**

[10] R.K. Amiet – *Acoustic Radiation From an Airfoil in a Turbulent Stream*, Journal of Sound and Vibration, 41 (4):407-420, **1975**

[11] K. Kucukcoskun, J. Christophe, C. Schram, J. Anthoine, M. Tournour – *An Extension of Amiet's Theory for Spanwise Varying Incoming Turbulence Noise and Broadband Noise Scattering Using BEM*, AIAA Paper 2010-3987, **2010**

[12] D. Fedala, S. Kouidri, F. Bakir, R. Rey – *Modeling of Broadband Noise Radiated by an Airfoil Application to an Axial Fan*, Int. Journal of Vehicle Noise and Vibration 3 (1), **2007**

[13] J. Christophe, J. Anthoine, P. Rambaud, S. Moreau – *Numerical Issues in the Application of an Amiet Model for Spanwise-Varying Incoming Turbulence*, AIAA Paper, 2008-2865, **2008**

[14] K. Kucukcoskun, J. Christophe, C. Schram, J. Anthoine, M. Tournour – *A Geometrical Near-Field Extension of Amiet's Theory for Spanwise Varying Incoming Turbulence Noise and Broadband Noise Scattering*, ISMA Paper 2010-690, **2010**

[15] Virtual Lab Rev 8: *User manual*, LMS International, **2008**

[16] C. Bailly, D. Juve, *Numerical Solution of Acoustic Propagation Problems Using Linearized Euler Equations,* AIAA Journal 38 (1):22-29, **2002**

[17] F. Gerard, M. Tournour, N. E. Masri, L. Cremers, M. Felice, A. Selmane – *Numerical Modeling of Engine Noise Radiation Through the Use of Acoustic Transfer Vectors: A Case Study*, SAE Paper, 2001-01-1514, **2001**

[18] K. Kucukcoskun, J. Christophe, C. Schram, M. Tournour – *A Semi-Analytical Approach on the Turbulence-Interaction Noise of A Low-Speed Axial Fan Including Broadband Scattering*, AIAA Paper 2011-2714, **2011**

[19] N. Curle – *The Influence of Solid Boundaries Upon Aerodynamic Sound*, Proc. R. Soc. London Ser. A, Vol. 231 (1187):505514, **1955**

[20] J. M. R. Graham – *Similarity Rules for Thin Aerofoils in Non-Stationary Subsonic Flows,* Journal of Fluid Mechanics 43: 753-766, **1970**

[21] M. Abramowitz, I. A. Stegun – *Han dBook of Mathematical Functions*, Dover Publications, **1972**

[22] M. Roger – *On Broadband Jet-Ring Interaction Noise and Aerofoil Turbulence-Interaction Noise Predictions*, Journal of Fluid Mechanics, 653:337-364, **2010**

[23] J. Christophe, J. Anthoine, S. Moreau – *Amiet's Theory in Spanwise Varying Flow Conditions*, AIAA Journal Technical Notes 47 (3), **2009**

[24] Y. Rozenberg – *Modelisation Analytique du Bruit Aerodynamique a Large Bande des Machines Tournantes: Utilisation de Calculs Moyennes de Mecanique des Fluides*, Ecole Centrale Lyon, 44, **2007**

[25] C. L. Morfey, H. K. Tanna – *Sound Radiation from a Point Force in Circular Motion, Journal of Sound and Vibration*, 15 (3):325-351, **1971**

[26] O. von Estorff – *Boundary Elements in Acoustics*, WIT Press, **2000**

[27] S. B. Pope – *Turbulent Flows*, Cambridge University Press, **2010**